PCCP

Accepted Manuscript

ROYAL SOCIETY OF CHEMISTRY

www.rsc.org/pccp

PCCP

RSCPublishing

ARTICLE

Gated Electron Transfer Reactions of Truncated Hemoglobin from *Bacillus subtilis* Differently Orientated on SAM-modified Electrodes

Cite this: DOI: 10.1039/x0xx00000x

Deby Fapyane[a], Andrey Kartashov[a], Claes von Wachenfeldt[b] and Elena E. Ferapontova[a]*

Received 00th January 2012,
Accepted 00th January 2012

DOI: 10.1039/x0xx00000x

www.rsc.org/

Electron transfer (ET) reactions of truncated hemoglobin from *Bacillus subtilis* (trHb-*Bs*) are suggested to be implicated in biological redox signalling and actuating processes that may be used in artificial environment-sensing bioelectronic devices. Here, kinetics of ET in trHb-*Bs* covalently attached via its surface amino acid residues either to COOH- or NH_2-terminated $(CH_2)_{2\text{-}16}$ alkanethiol SAM assembled on gold are shown to depend on the alkanethiol length and functionalization, being not limited by electron tunnelling through the SAMs but gated by ET preceding reactions due to conformational changes in the heme active site/at the interface. ET gating was sensitive to the properties of SAMs trHb-*Bs* interacted with. The ET rate constant k_s for a $1e^-/H^+$ reaction between the SAM-modified electrode and heme of trHb-*Bs* was 789 and 110 s^{-1} after extrapolation to a zero length SAM, while the formal redox potential shifted 142 and 31 mV, for NH_2- and COOH-terminated SAMs, correspondingly. Such domain-specific sensitivity and responsitivity of redox reactions in trHb-*Bs* may be of immediate biological relevance and suggests the existence of bioelectronic regulative mechanisms of ET proceeding *in vivo* at the protein-protein charged interfaces that modulate the protein reactivity in biological redox signalling and actuating events.

1. Introduction

Biological electron transfer (ET) reactions, linked to cellular life maintenance processes, are performed by ET proteins and enzymes and represent one of the most sophisticated for understanding and mimicking bioelectronic events.[1] Hitherto, most efforts were focused on understanding long-range ET underlying such crucial for life and biotechnologically challenging bioenergetic phenomena as respiration and photo-synthesis.[2-5] Recently, biological sensor-and-actuator systems started to attract more attention, in particular, those constituted of heme proteins and enzymes,[6-8] the acquired knowledge shedding some light on complex mechanisms by which organisms receive information on environmental changes and adaptively respond to it. Modes of binding of messenger molecules, their activation and transport, allosteric regulation of processes, and conformational and redox properties of the proteins may be implicated in signal receiving and messaging.[6, 7, 9]

Bacterial truncated hemoglobins (trHbs) are proteins supposedly involved in oxygen and other ligand sensing reactions and signal transduction in bacteria, though their precise role, in contrast to bacterial flavohemoglobins and already characterized heme-containing chemotactic sensors, is not well understood yet.[10-14] It is however clear that their involvement in cellular sensing and signalling should be exhibited and regulated via ET reactions with signalling and messaging species, and include intimate interactions between the protein partners linked to their functioning and folding, the same way as in other biological ET systems. Study of these ET reactions and their correlation with biological ET can be performed electrochemically, once a direct electronic communication between a protein and an electrode is established.[15-18] TrHbs, with their small molecular size resulting from truncated amino acid sequences,[11,12,14] can establish such direct electronic contact with electrodes, and that allows direct electrochemical interrogation of their ET and ligand binding properties.[19] Redox reactions of ~15 kDa trHb from the gram-positive soil bacterium *Bacillus subtilis* (trHb-*Bs*) adsorbed on graphite (Gr) were shown to be tuned by ligand binding, and ET was fast enough for the development of one of the most efficient Hb bioelectrocatalysts for oxygen reduction, characterized by the apparent catalytic rate constant, k_{cat}, of 56 s^{-1}.[19] Along with that, uncontrollable, random immobilization of the protein on Gr, shown also for several other heme proteins and enzymes,[20-22] resulted in generally moderate ET rates between the electrode and heme of trHb-*Bs* and did not provide enough knowledge about protein-electrode interactions and possible ways of their

modulation to achieve faster ET rates. The latter is critical for analysis of protein ET reactions with short-living ligands biology often uses as messengers of environmental changes.[23] A more controllable orientation of heme proteins can be achieved by protein immobilization on metal electrodes via genetically encoded tags with high affinity for gold and silver[24-29] and by electrostatically favoured coupling to functionalized self-assembled monolayers (SAM) of alkanethiols.[26, 27, 30-33] The ET reaction rates orders of magnitude faster than on Gr has been achieved,[34] and thus these approaches can be considered as the most straightforward way for optimization of ET of proteins at the electrode/solution interface.

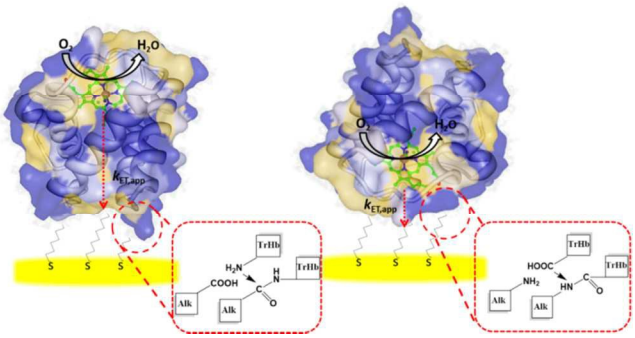

Figure 1. Schematic representation of the electrode modification by trHb-*Bs* covalently attached to (left panel) COOH- and (right panel) NH_2- terminated alkanethiol SAMs on gold.

To achieve electrostatic and structural compatibility requested for the most efficient ET functioning, the modified electrode surface is expected to mimic the surface properties of protein biological partners. Functionalised SAMs of alkanethiols on metal electrodes were shown to provide biocompatible surfaces for ET reactions of such heme proteins and enzymes as cytochrome *c* (cyt *c*),[24, 35-38] sulphite and theophylline oxidases, [30, 33, 39] and some other complex proteins,[17] then properly oriented at the electrodes. Such SAMs represent easily controllable model systems for studies of the effects of charged interfaces formed by binding domains of interacting proteins on ET reactions, sensitive to minor changes in the composition and length of the alkanethiols used. [24 26, 33, 40]

Here, to address the biological functioning of trHb-*Bs* related to environmental redox sensing and transmission,[7, 41, 42] its ET reactions were electrochemically interrogated at functionalized alkanethiols self-assembled on gold electrodes. In trHb-*Bs*, the five-coordinated heme iron is axially coordinated to the imidazole nitrogen of the proximal H76 histidine, and the ferric iron-histidine nitrogen distance of 1.91 Å is unusually short compared to any other heme-proteins.[10] Such tight coordination to His known for its electron donating properties as well as a well-developed solvent channel to the heme pocket may be responsible for a quite low heme potential in trHb-*Bs*[43, 44] approaching that of free hemin.[45] The redox potential of the trHb-*Bs* heme, both in solution and when it is adsorbed on Gr, is around -330 mV at pH 7.[19] In the reduced state, the sixth coordination position of heme iron is occupied by O_2, which is displaced by water or any other ligand molecule in anaerobic conditions and/or in the oxidized ferric state. Ligation of the heme iron has been shown to dramatically affect ET properties of the protein,[19] and it might be expected that ET reactions of trHb-*Bs* could be environmentally modulated in response to any other relevant environmental changes. Since these ET reactions generally proceed at the interface formed by the contacting domains of trHb-*Bs* and its partner molecule, they were studied in trHb-*Bs* covalently attached to differently functionalized alkanethiol SAMs, bearing COOH- and NH_2 terminal groups. We aimed at finding conditions for the fastest ET enabling analysis of short-living ligands and elucidation of possible ET pathways and mechanisms of ET in trHb-*Bs* differently orientated at the SAM-modified electrodes via either its cationic or anionic domains.

2. Experimental

2.1 Materials

TrHb-*Bs* (MW 15 kDa) was produced as previously described.[19] 16-Amino-1-hexadecanethiol ($C_{16}NH_2$); 11-amino-1-undecanethiol ($C_{11}NH_2$), 8-Amino-1-octanethiol (C_8NH_2), 6-amino-1-hexanethiol (C_6NH_2), 2-amino-1-ethanethiol (C_2NH_2), 16-mercaptohexadecanoic acid ($C_{15}COOH$); 11-mercapto-undecanoic acid ($C_{10}COOH$), 11-mercaptoundecanol ($C_{11}OH$), N′-ethylcarbodiimide hydrochloride (EDC·HCl), N-hydroxy-succinimide (NHS), and the components of buffer solutions were from Sigma Aldrich (Broendby, Denmark). Milli-Q water (18 MΩ, Millipore, Bedford, USA) was used. 6-Mercapto-hexanoic acid (C_5COOH) was from Dojindo Laboratories, Kumamoto, Japan.

2.2 Methods

Electrode modification. Rods of solid spectroscopic graphite (SGL carbon AG, Werk Ringsdorff, Germany, type RW001, 3.05 mm diameter, geometric surface area of 0.071 cm^2, roughness factor of 10)[22] were cut and fitted into the home made Teflon holders. This way produced Gr electrodes were polished on a silicon carbide emery paper (SIC 1000, Ballerup, Denmark), then rinsed thoroughly with Milli-Q water and dried in an N_2 flow. For protein adsorption, 3 µl of a 1.8 mg ml^{-1} protein solution were placed on the Gr surface and kept for 3 h at 4°C under a plastic lid.

Gold electrodes (CH instruments, Austin, TX; diameter 2 mm) were cleaned by potential cycling in 0.5 M NaOH (from 0.4 to -1.6 V, scan rate 0.1 V s^{-1}, 10 cycles) and successively mechanically polished in a 1 µm diamond and 0.1 µm alumina slurries (both from Struers, Copenhagen, Denmark). After mechanical polishing, the electrodes were ultrasonicated for 5 min in a 1:1 water-ethanol mixture and electrochemically polished in 1 M H_2SO_4 (from -0.3 to 1.7 V, scan rate 0.3 V s^{-1}, 10 cycles) and 1 M H_2SO_4 containing 1 mM KCl (from 0 to 1.7 V, 0.3 V s^{-1}, 10 cycles), respectively. The surface area of electrodes, determined from the gold oxide reduction peak in 0.1 M H_2SO_4, was 0.085 ± 0.007 cm^2. Clean electrodes were

rinsed thoroughly with Milli-Q water and kept in absolute ethanol for 30 min prior to modification. For SAM formation, the gold electrodes were kept in 1 mM solution of the corresponding alkanethiol in ethanol (20 mM in the case of C_2NH_2) overnight (~16 h), and for 40 h for $C_{16}NH_2$ and $C_{15}COOH$. The SAM-modified gold electrodes were rinsed with ethanol, Milli-Q and dried gently in the N_2 flow. TrHb-*Bs* was covalently coupled to the NH_2-terminated SAM modified gold electrodes by carbodiimide chemistry,[45, 46] by placing 4 µl of a mixture of EDC·HCl and trHb-*Bs* (final concentrations of 100 mM EDC·HCl and 0.9 mg ml^{-1} protein) in 10 mM phosphate buffer solution (PBS), pH 5.5, on the SAM-modified surface, left to react for 3 h. Before measurements, trHb-*Bs*-modified electrodes were carefully washed in 10 mM PBS, pH 5.5, to remove the unbound protein. Prior to coupling, COOH- and OH-terminated SAM were activated by keeping SAM-modified electrodes in a mixture of 75 mM EDC·HCl and 25 mM NHS (final concentrations) in 10 mM PBS, pH 5.5, for 3 h at r.t. The activated electrodes were rinsed in PBS and modified by 4 µl of 0.9 mg ml^{-1} trHb-*Bs* solution in 10 mM PBS, pH 7.5, allowed to react for 1 h at 4°C (20 h for $C_{15}COOH$).

Instrumentation and procedure. Cyclic voltammetry (CV), differential pulse voltammetry (DPV), and square wave voltammetry (SWV) were performed in a standard three-electrode electrochemical cell connected to a µAutolab potentiostat (Type III, Eco Chemie B.V., Utrecht, Netherlands) supported with GPES (version 4.9) and NOVA (Type 1.8.17) software. An Ag|AgCl (3 M KCl) electrode and a Pt wire were the reference and auxiliary electrodes, correspondingly. All electrochemical measurements were carried at 20±1°C in 10 mM PBS, pH 7.0, deaerated by Ar for 1 h, unless specified otherwise. In DPV, the modulation amplitude was 25 mV, modulation time: 50 ms, interval time: 0.2 s, and step potential: 1 mV. SWV was performed within the 400 - 3 Hz frequency range, with pulse amplitude of 25 mV and step potential of 1 mV. The kinetic parameter in SWV analysis, κ_{max}, was 1.19.[47]

Theoretical analysis of ET rates within the protein structure. A theoretical analysis of ET rates within the protein structure was performed by the program for calculation of ET rates in proteins.[48] The approach exploits the semi classical Marcus ET theory and determines the ET rate constant k_{ET} (in s^{-1}) as a function of the distance, r, between the redox centres, the change of the free energy ΔG^o (predetermined by the redox potential difference) and reorganization energy, λ, reflecting the structural rigidity of the redox centres at the atomic level:[49]

$$k_{ET} = k_0 \exp[-\beta(r)] \exp[-((\Delta G^0 + \lambda)^2 / 4\lambda kT)] \quad (1)$$

Here, β is a tunnelling parameter of the electronic coupling with r, k is the Boltzmann constant, T the temperature. Since the ET distance/pathway crucially affect the ET rate, both through r and β and variations in the polypeptide structure accounting for β variations, the contribution of the intervening medium to the ET rate were addressed by taking into account the packing density of the protein atoms, ρ, in the space between the protein redox centre and the electrodes estimated by analysis of the 3D trHb-*Bs* structure,[10] which transformed Eq. (1) to the one used for the k_{ET} estimations:[48]

$$\log_{10} k_{ET}^{exorgenic} =$$

$$= 13.0 - (1.2 - 0.8\rho)(R - 3.6) - 3.1(\Delta G + \lambda)^2/\lambda \quad (2)$$

Here, R is the edge-to-edge distance (in Å) between the electrode (the chosen surface atom) and the heme iron; the rate constants were estimated for $\Delta G_{opt} = -\lambda$.[48] The variations in ρ defined as the fraction of the volume between redox centres that is within the united van der Waals radius of intervening atoms were taken in to account by the ρ weighting term $(1.2 - 0.8\rho)$.[48]

3. Results and discussion

ET between proteins and electrodes was shown to critically depend on the protein orientation onto electrodes, the favourable orientations providing the electron tunnelling pathways with the highest ET rates.[17, 26, 36, 38, 50, 33] Here, to orient the protein properly for the most efficient ET, trHb-*Bs* was covalently attached to functionalized alkanethiol SAMs by carbodiimide coupling of the COOH- and NH_2-functionalities of its surface amino acid residues to the NH_2- and COOH-terminal groups of SAMs (Figure 1).[46] This coupling reaction was not expected to affect the structural integrity/conformation of the protein,[51] but, in low ionic strength solutions, provide orientations of trHb-*Bs* onto the SAM-modified electrodes through either positively or negatively charged protein surface domains. Those electrostatically controllable orientations could be advantageous over statistically random orientations of trHb-*Bs* on Gr and provide information on kinetics of ET in a more addressable and electrostatically controllable way. ET reactions of trHb-*Bs* on positively and negatively-charged SAM surfaces were electrochemically analysed and used for correlations with the possible ET pathways within the protein structure.

3.1 Electrochemistry of trHb-*Bs* covalently coupled to SAM-modified gold electrodes

In agreement with the previous results,[19] trHb-*Bs* physically absorbed on Gr demonstrated a distinct couple of peaks with a formal redox potential, E^0, of around -330 mV, consistent with the redox transformation of its heme active site (Figure 2A, Table 1). Adsorption on Gr did not notably affect the native conformation of the protein, and the determined E^0 was similar to that shown in solution.[19] The heterogeneous ET rate constant, k_s, estimated both by the Laviron[52] and Komorsky-Lovrić-Lovrić formalisms[47] levelled at moderate 7-8 s^{-1} (Table 1). A more efficient ET was targeted with trHb-*Bs* covalently attached to the alkanethiol SAMs bearing oppositely charged terminal groups; the effect of the electrostatically assisted orientations on the k_s has been evaluated.

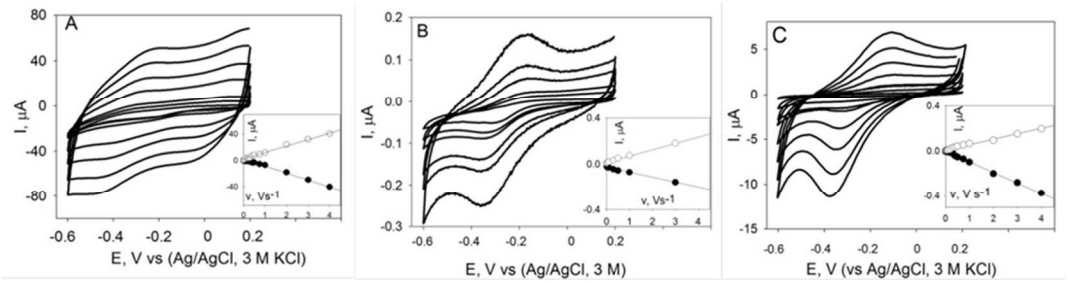

Figure 2. Representative CVs recorded in deaerated 10 mM PBS, pH 7.0, with trHb-*Bs*–modified (A) Gr and (B) C_{10}COOH- and (C) $C_{11}NH_2$–SAM modified gold electrodes. Potential scan rate v varied between 0.01 to 5 V s^{-1}. Insets: Dependence of the CV peak currents on v.

A well-defined couple of redox peaks at potentials approaching those of trHb-*Bs*'s heme could be followed in CVs of trHb-*Bs* covalently attached to C_{10}COOH and $C_{11}NH_2$ SAM-modified gold electrodes (Figure 2B,C) and less developed for C_{11}OH, where carbodiimide coupling appeared be inefficient (Figure S1, ESI). A slight asymmetry of peaks can be related to the involvement of a protonation step in the overall ET reaction.[53] The CV peak currents, I_p, were linearly proportional to the potential scan rate, v, consistent with the heterogeneous ET in the adsorbed layer.[54] Compared to the E^0 characteristic for trHb-*Bs* on Gr (Figure 2A), the E^0 of the heme in trHb-*Bs* attached to the SAMs shifted 20-25 mV in the less negative direction both for C_{10}COOH, $C_{11}NH_2$ and C_{11}OH SAMs (Table 1). Similar (~25 mV) potential shifts in the positive direction were also reported for cyt *c* bound to the COOH-SAM-modified electrodes versus quite hydrophilic tin oxide electrodes[24] and may be attributed to different electrochemical properties of the electrodes, such as the potential of zero charge[55] and the electric field strength resulting from the different structure of the electric double layer, EDL, on the SAM surface.[56]

ET reactions of trHb-*Bs* were also interrogated on NH_2- and COOH-functionalized shorter alkanethiol SAMs (Figures S1 and S2, ESI). The covalent attachment of trHb-*Bs* to the NH_2-terminated SAMs resulted in the generally decreased surface coverage of the electroactive protein, approaching 30-50% of the monolayer, while on the COOH-terminated SAM electrodes trHb-*Bs* surface density approached the monolayer one (Table 1). Incomplete monolayer formation may be referred either to the protein-electrode coupling reaction less efficient on the NH_2-terminated SAMs or to the presence of trHb-*Bs* with orientations improper for the efficient direct ET reaction and thus not providing electrochemical noticeable signal. For COOH-terminated SAMs all orientations of trHb-*Bs*, via positively charged domains, evidently resulted in the electroactive protein monolayer. Another important tendency that could be followed is the increasing shift of the heme redox potential to less negative values upon decreasing the alkane chain length, particularly pronounced for NH_2-functionalized SAMs (Table 1). The magnitude of the potential shift (up to 120 mV) could not be ascribed to general EDL effects and will be discussed in detail after kinetic analysis of the ET process.

3.2 Analysis of ET rates

The k_s for ET between the SAM-modified gold and heme of trHb-*Bs* coupled to functionalized SAMs was first evaluated by the Laviron approach from the CV peak potentials difference. However, processing of the CV peaks, becoming broader at higher potential scan rates and being insufficiently developed for lower protein surface coverages, resulted in distorted Laviron trumpet plots, which did not allow precise determination of ET rates for some of the SAMs. Therefore, the ET rate constants were estimated from the SWV data (Figure S3, ESI) by the Komorsky-Lovrić-Lovrić method, by constructing dependences of the SWV peak currents, I_p, related to the frequency at which they were measured, on the measurement frequency (Figure 3) exhibiting a maximum at a frequency that directly relates to the k_s:[47]

$$k_s = \kappa_{max} \times f_{max} \qquad (3)$$

Here, the κ_{max} is the tabulated kinetic parameter that depends on the transfer coefficient α and the product of $n_e E_{sw}$ (E_{sw} is the square-wave amplitude and n_e is the number of electrons transferred). This approach has demonstrated its advantage in kinetic ET analysis of minute surface amounts of proteins[29] and ET reactions of weakly adsorbed species.[57-59]

The SWV analysis of ET kinetics evidenced that ET in trHb-*Bs* covalently attached to the SAM-modified electrodes generally proceeded with reaction rates higher than those on Gr (Table 1), and the ET rate constants consistently increased for shorter SAMs, for which the electron tunnelling distance along the alkane chain decreased.[31, 36, 60] Also, higher ET rates could be followed with trHb-*Bs* covalently linked to shorter NH_2-terminated SAMs as compared to COOH-functionalized SAMs (Figure 3, Table 1). Faster ET on NH_2-SAM might implied that orientations of trHb-*Bs* interacting with the electrode surface via its negatively charged domains provided more efficient ET pathway between the heme moiety and the protein surface amino acid residues coupled to the amine terminal groups of SAMs.

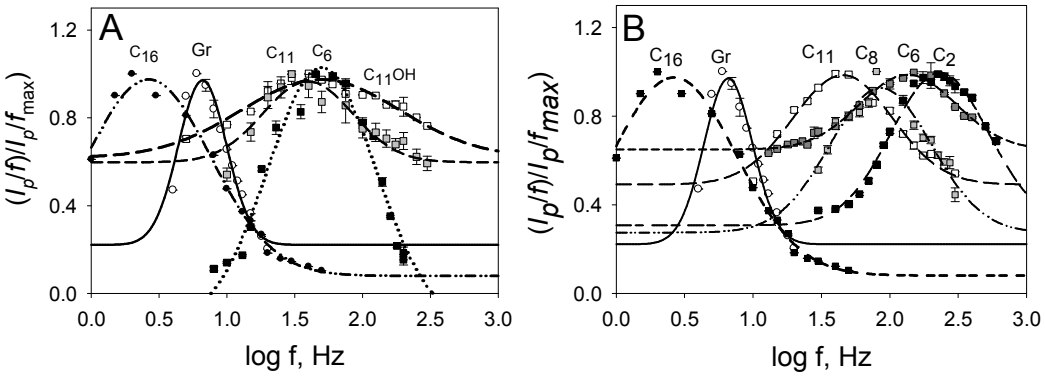

Figure 3. Dependences of the normalized ((I_p/f)/(I_p/f_{max})) peak currents on the logarithmic frequency, constructed from the SWV recorded with trHb-*Bs*-modified electrodes; (A) Gr and $C_{11}OH$-, $C_{15}COOH$-, $C_{10}COOH$-, C_5COOH-SAMs, and (B) Gr and $C_{16}NH_2$-, $C_{11}NH_2$-, C_8NH_2-, C_6NH_2- and C_2NH_2- SAMs

To validate this hypothesis, contributions from the electron tunnelling through the SAM and intramolecular ET to the overall ET rate were estimated.

Table 1. Surface coverage, formal potentials and ET rate constants determined for trHb-*Bs* adsorbed on Gr and covalently attached to the SAM-modified gold electrodes

Electrode	Γ, pmol cm^{-2} [a]	E^0_{DPV}	E^0_{SWV}	$k_{s\,SWV}$, s^{-1}
Gr	22.0 ± 6.0	-329 ± 8	-332 ± 3	8.0 ± 0.8
$C_{15}COOH$	1.03±0.3.	-323± 6	-311± 4	1.2± 0.2
$C_{10}COOH$	14.2 ± 1.2	-310 ± 5	-305 ± 3	37.8 ± 2.0
C_5COOH	15.4 ± 0.98	-298 ± 1	-285 ± 2	61.4 ± 1.0
$C_{11}OH$	3.0 ± 0.2	-309 ± 4	-309 ± 2	46.6 ± 2.0
$C_{16}NH_2$	1.1±0.4.	-318 ±5	-313± 4	2.0± 0.5
$C_{11}NH_2$	5.0 ± 0.9	-303 ± 2	-309 ± 2	45.5 ± 3.0
C_8NH_2	4.9 ± 0.5	-260 ± 4	-292 ± 2	99.4 ± 1.0
C_6NH_2	9.8 ± 0.4	-216 ± 1	-234 ± 4	159.9 ± 2.0
C_2NH_2	5.9 ± 1.4	-187 ± 1	-240 ± 5	282.3 ± 8.0

[a] - data are referred to the electrode surface area accounting for the surface roughness.

3.3 Deconvolution of intramolecular and intermolecular ET rates

Intramolecular ET rates within the protein ($k_{ET,app}$) were evaluated according to the model considering three steps of ET: intramolecular ET from the heme to the amino acid group at the protein surface, intermolecular ET from this group to the terminal groups of SAM (in our case represented by the carbodiimide bond) and intermolecular electron tunnelling through the alkane chains of SAMs.[36] Practically, deconvolution was performed by plotting the natural logarithm of the heterogeneous ET rate constant (ln k_s) versus the number of C-C bonds in the SAM-constituting alkanethiol (Figure 4).

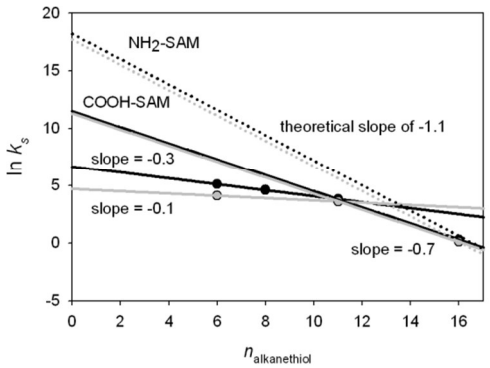

Figure 4. Dependence of the heterogeneous ET rate constant, k_s, (logarithmic scale) on the number of methylene groups in the alkane chains of SAM, $n_{alkanethiol}$. Solid and dotted lines show experimental and theoretically expected dependences of ET rates on the length of the alkanethiol chain (for n>6), for trHb-*Bs* covalently attached to (black) NH_2-SAMs and (grey) COOH-SAMs.

Theoretically, if ET is limited by electron tunnelling through the SAM (for the methylene group number n > 6) the exponential decay of the ET rate constant with the increasing number of C-C bonds is expected:[31, 36, 60]

$$k_s = k_{(n=0)} \exp(-\beta n) \qquad (4)$$

where n is the number of methylene groups, the tunnelling decay factor β ranges between 1.0 and 1.1.[26, 31] Extrapolation of the ln(k_s) on n dependence to n =0 then gives the value of the ET rate constant in the absence of SAM, namely, exclusively through the protein matrix.

As can be seen from Figure 4, electron tunnelling through the SAMs appears not to be the limiting step: the experimental slopes of the ln(k_s)-n dependences do not follow Eq.(2) and are essentially lower than theoretically predicted (dotted lines). Even for long C11-C16 alkanethiols, the dependence does not fit this model, and the ET reaction rate seems to be limited by some non-ET process. Protein conformational changes prior or

concomitant to the ET reaction and protonation-deprotonation steps may contribute to the observed "apparent" ET rates:[61] when ET becomes fast enough they start to limit the overall reaction rate. Protein conformational reorganisation at the electrode/solution interface[62] and proton transfers coupled to the ET reaction[29] as a rate limiting step thus can be considered. Therewith, based on the unprecedented variation of the heme redox potential in the studied system, particularly pronounced for short alkanethiols (Table 1), strong changes in the protein active site, not at the interface, may be suggested to gate the ET process.[62]

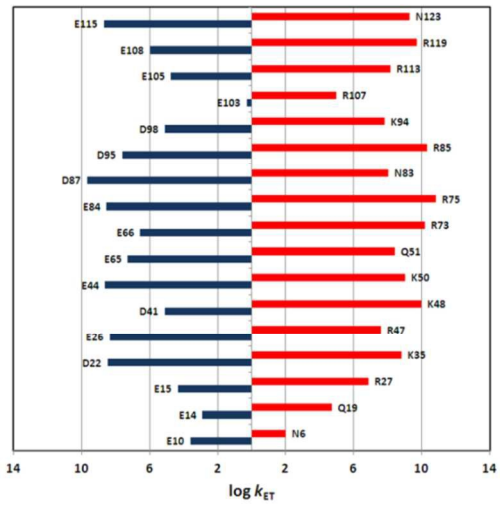

Figure 5. Theoretical rates of intramolecular ET ($k_{ET, app}$) from the heme moiety to the protein surface-exposed amino acid groups of trHb-*Bs*. (Blue) Left panel and (red) right panel represent -COOH and -NH_2 possessing surface amino acid residues, respectively (for more details see ESI, Table S1)..

On short SAMs, such gated ET appears to be slower for trHb-*Bs* interacting via its positively-charged NH_2-bearing domains with negatively charged COOH-SAMs (Figure 4, Table 1, for C6 more than two-fold difference in values). However, if we assume that on C16 SAMs the electron tunnelling through the SAM becomes a limiting step, then the theoretical ET rates $k_{ET,(app)}$ through the protein, in the absence of alkanethiols, reach 8.1×10^5 and 9.8×10^5 s^{-1}, for COOH- and NH_2- terminated SAM, correspondingly (extrapolation of theoretical dotted lines in Figure 4 to n=0). Those values are close and suggest that in the absence of electrified interface-induced variations, ET rates for different protein orientations may be similar and quite fast.

Theoretical ET rates between the heme and correspondingly charged protein surface amino residues were also calculated by the Dutton model.[48, 49] They show a quite similar pattern of the ET rates distribution (Figure 5), though, with a statistically larger number of positively charged amino acid residues providing ET rates within (or exceeding) 10^6 s^{-1} (extrapolation limits in Figure 4, dotted lines). Thus, the theoretical $k_{ET, app}$ values do not allow immediate correlations with trHb-*Bs* orientations at the modified electrodes via some specific amino acid residues involved in the coupling reaction, but rather with their broad distribution.

Thus, on shorter SAMs, a clear distinction in ET properties of differently oriented trHb-*Bs* can be followed. Extrapolation of the experimental k_s values obtained with COOH- and NH_2-terminated SAMs to n=0 gave the $k_{(n=0)}$ for gated ET of 110 and 789 s^{-1}, correspondingly. Those values reflect stronger effects of interfacial interactions and EDL on intramolecular ET rates in trHb-*Bs* coupled to the electrodes via its positively charged amine groups. From general point of view, it may be discussed in terms of different conformational sensitivities and bioelectronic responsitivity of the protein attached to either COOH or NH_2 groups of a SAM-modified electrode to the processes proceeding at the charged interface, which may be of a biological significance.

3.4 Redox potential of trHb-*Bs* covalently coupled to SAMs of different lengths

A significant shift of the heme potential could be followed for trHb-*Bs* covalently coupled to the SAMs of continuously decreasing lengths (Table 1). The redox potential of trHb-*Bs* adsorbed on graphite, -329 mV (DPV measurements), demonstrates the same value as in its native state in solution and thus can be considered as a reference value for the conformationally undisturbed protein.[19] Even with C16-SAMs the trHb-*Bs* potential does not approach that value and unprecedentedly shifts in the positive direction upon decreasing the alkanethiol chain length. This shift can be seen for both protein orientations and is larger for the positively charged SAMs (for C6, 113 mV on NH_2-SAMs *vs*. 31 mV on COOH-SAMs, DPV data), for which higher gated ET rates are observed (Table 1).

In general, formal potentials of redox species can vary as a function of such conditions as surface coverage, electrolyte nature, lengths and nature of SAMs, and some other. Imbedding of the ferrocenium cation (Fc) into the less polar SAM environment was reported to result in a 130 mV formal potential shift,[63, 64] ascribed to the ion solvation and EDL effects.[63] Unless the polarity changes, a very moderate and statistically insignificant variations of Fc redox potentials were observed on C10-C3 SAMs,[65] with the only up to 10 mV SAM-related potential drop in the EDL.[66] Similarly small potential changes associated with a shorter alkanethiols were observed for the ET protein, cyt *c*, covalently attached to COOH-terminated C16-C5 SAMs.[24, 67, 68]In proteins, redox potentials may change as a function of the solvent exposure (e.g. protein unfolding) and heme ligation.[43, 44] Heme in trHb-*Bs* is already solvent exposed (Figure 6C) and such solvent accessibility should be responsible for a quite low heme redox potential approaching that of free hemin.[45] Another factor affecting the heme potential in trHb-*Bs* is heme coordination to the proximal His ligand that plays an important role in heme stabilization. Compared to other amino acid residues, His is considered as a good electron donor that stabilizes the Fe^{3+} oxidation state and shifts the heme redox potential to more negative values.[43] Additionally, in trHb-*Bs*, heme coordination to its proximal His-F8 (Figure 6A) is characterized by the unusually (compared to other bacterial Hbs) short distance of about 1.91 Å.[10, 69, 70]

Any perturbations in the heme coordination state, such as those affecting the distance between the heme iron and nitrogen of the His imidazole ring, can be expected to decrease the extra electronic density on the iron atom and shift the highly negative redox potential trHb-*Bs* to less negative values.

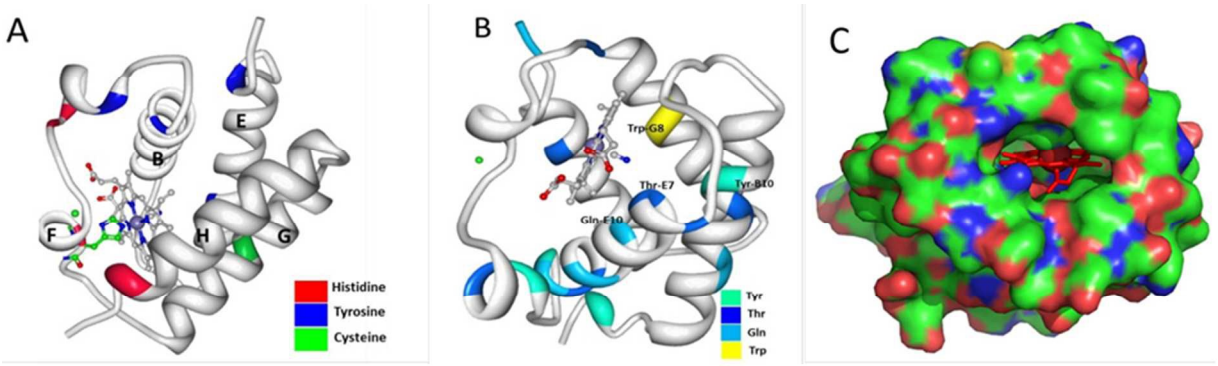

Figure 6. 3D-structures of trHb-*Bs* (PDB files ID: 1ux8)[10], highlighting (A) His-F8 as a heme proximal ligand; (B) ligand-inclusive hydrogen bond network (LIHBN) in the heme distal region, and (C) Surface representation: (red-coloured domains) positively charged and (blue-coloured domains) negatively charged amino acid residues; heme is denoted in red. A solvent exposed channel into the heme pocket is clearly seen.

In this context, protein misfolding that would result in the increased hydrophobicity of the protein interior and less solvent exposure of the heme is less probable. The active site of trHb-*Bs* is surrounded by the extremely rigid polar distal environment, for which changes in the polarity are not expected. This environment is also referred to as a ligand-inclusive hydrogen bond network (LIHBN) formed by coordination of the neighbouring amino acid (Trp^{89}-G8) indolic nitrogen to the heme[10] (Figure 6B). Both solvent exposure of the heme and the trHb-*Bs*' LIHBN would require strong and possibly nonspecific stimuli for their disruptions in order to increase the hydrophobicity of the trHb-*Bs* interior in the vicinity of heme.

As most of bacterial trHb, trHb-*Bs* is extremely stable against nonspecific environmental changes, with its globin-like fold protecting heme from rapid oxidation and overall excellent storage stability.[12] Its misfolding at differently charged interface seems to be less probable than minor changes in the His-heme coordination that may nevertheless produce strong changes in the heme redox potential. For example, the His instead of Met coordination in *c*-type cytochromes may be associated with 292-733 mV negative shift in the heme potential.[43]

Thus, if the shift of the trHb-*Bs* redox potential results mostly from changes in the heme ligation to His, induced by specific electrostatic interactions and EDL effects at the protein | SAM-modified electrode interface, then this may be also assessed by analysing the heme iron protonation reaction coupled to ET (Eq. 5). More specifically, since trHb-*Bs*' heme is strongly coordinated to the proximal His-F8,[11, 14] this His should be primarily involved in its stabilization and protonation. Then, any changes in the coordination distance are very likely to affect the protonation reaction and this can be followed by analysis of the pK_a of the residue involved in the redox reaction.

3.5 Effect of the pH on the formal redox potential of the heme in *trHb-Bs*

The $Fe^{2+/3+}$ redox transformation of the five-coordinated heme redox centre is commonly associated with a concomitant proton transfer,[21, 53] and for trHb-*Bs* immobilized on Gr, the pH dependence of the heme redox potential (in basic and neutral solutions) is consistent with a $1e^-/1H^+$ redox reaction:[19]

$$\text{trHb-}Bs\ (Fe^{3+}) + e^- + H^+ \leftrightarrow \text{trHb-}Bs\ (H^+\text{-}Fe^{2+})\ (5)$$

A slope of -60 mV/pH observed in basic and neutral solutions changed to -30 mV/pH at pH below 7 (Figure 7A), consistent with a change of the $1e^-/1H^+$ to $1e^-/0.5H^+$ transfer mechanism in acidic solutions and the pK_a of the amino acid residue presumably involved in the reaction, His-F8, of 7. Interestingly, for the $C_{15}NH_2$ SAM, data close to those on Gr were obtained (ESI, Figure S5).

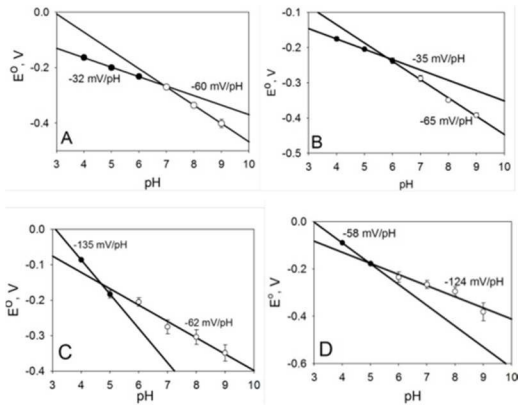

Figure 7. pH dependences of the heme redox potential in trHb-*Bs* immobilized on (A) Gr, (B) $C_{11}NH_2$, (C) C_6NH_2 and (D) C_2NH_2 modified gold, DPV (Figure S4, ESI) were recorded in deaerated 10 mM PBS of the corresponding pH.

For trHb-*Bs* attached to the $C_{11}NH_2$ SAM, a minor potential shift to less negative potentials could be correlated with the pK_a

changing from 7 to 6. The redox potential shifted further to less negative potentials in trHb-*Bs* coupled to C_6NH_2 and C_2NH_2 SAMs was consistent with a further decrease of the pK_a to 5 (Figure 7B-D). Apparently, the proton donor ability of His-F8 decreases with the decreasing length of the SAM the protein is attached to, and this should also contribute to the decreasing ET rates now apparently becoming gated by the proton transfer reaction. What is particularly interesting, the slope of the E^o-pH dependences, for such a short alkanethiol as C2, appears to be very different from -60 mV/pH observed with Gr and long SAM-modified electrodes, approaching -120 mV/ pH, which theoretically correlates with the change of the reaction mechanism, from $1H^+$ to $2H^+$ involved per one electron transfer (Figure 7D) and strongly implies that the mode of the proton involvement in the ET reaction changes.[10-14d] Considering the complexity of the ET reaction, additional conformational changes associated with the proton and electron transfer process can be anticipated.[32]

3.6 Electrocatalytic reduction of O_2 by trHb-*Bs* attached to SAM-modified electrodes

The detected shift in the heme redox potential and variations in ET rates of trHb-*Bs* attached to differently charged SAMs of varying lengths should also affect ligand recognition, its binding in the heme distal pocket and transformation by trHb-*Bs*. In particular, minor variations in the LIHBN (in they did occur) were expected to affect the O_2 binding in the heme distal pocket and thus might reveal polarity changes in the trHb-*Bs* interior. Thus, the electrocatalytic reduction of O_2 by trHb-*Bs* attached to the SAMs has been studied.

Bioelectrocatalysis of O_2 reduction generally occurs via the O_2-heme binding step followed by oxidation of the ferrous heme to its ferric state in the $4e^-/4H^+$ reaction with dioxygen:[19]

$$\text{trHb-}Bs(Fe^{2+}) + O_2 \rightarrow \text{trHb-}Bs((Fe^{2+})\text{-}O_2) \quad (6)$$

$$\text{trHb-}Bs((Fe^{2+})\text{-}O_2) + 4e^- + 4H^+ \rightarrow$$

$$\rightarrow \text{trHb-}Bs(Fe^{2+}) + 2H_2O \quad (7)$$

where heme is reduced to its ferrous state by the electrode (four electrons in Eq.(7) are donated by the electrode). For simplicity of presentation, the protonation reaction (Eq. 5) is not depicted in Eq. (6),(7), but it always proceeds once the heme is reduced to its ferrous state.

Bioelectrocatalytic reduction of O_2 by trHb-*Bs* starts at around -0.1 - -0.2 V, depending on the corresponding redox potential of trHb-*Bs*' heme on different SAMs (Figure 8), and is a characteristic reaction of five-coordinated heme in proteins and enzymes.[19, 30, 71] Electroreduction of O_2 at bare Gr also starts at relatively high potentials though with a much lower efficiency than that observed in catalysis by trHb-*Bs*.[19] SAMs are known to block the reaction of O_2 electroreduction on gold, which then starts at -0.2 - -0.4 V (depending on the alkanethiol length) and with efficiency even lower than that on Gr (Figure S6, ESI).

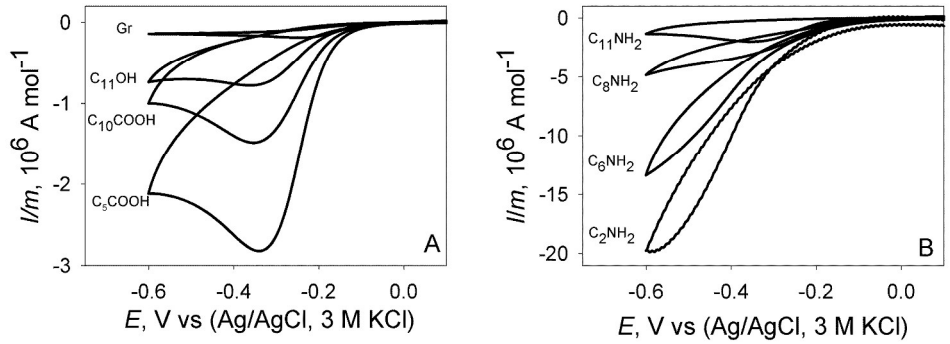

Figure 8. Representative background-corrected CVs of O_2 reduction by trHb-*Bs* immobilised on (A) graphite, OH-, COOH- and (B) NH_2-terminated SAM modified gold electrodes, recorded in 10 mM PBS, pH 7.0, unstirred solutions, and normalized for the protein surface amount, *m*, in pmoles. Potential scan rate 50 mV s^{-1}.

The most efficient bioelectrocatalysis (in terms of specific currents, i.e. referred to the amount of the catalyst) was observed at the electrodes characterized by the fastest ET rates, i.e. on the short-length alkanethiol SAMs, in agreement with the k_s values obtained (Table 1, Figure 8). Along with that, the general waveform of the reduction waves was somehow inconsistent with the apparent efficiency of the process and allowed several qualitative conclusions on the O_2 binding in the trHb-*Bs* active site.

More specifically, a peak-shaped bioelectrocatalytic CVs could be followed on Gr, C11 and COOH/OH SAMs, i.e. SAMs on which either insignificant or minor changes of the heme redox potential occurred (Figure 8). Such a peak-shape dependence can be correlated either with certain O_2 diffusion limitations (consistent with the dependence of the catalytic currents on the electrode rotation such as on Gr, which absolute loading with the protein was at least order of magnitude higher than that of SAM-modified electrodes)[19] or the presence of the reaction limiting steps different from the ET itself.[72-74] Otherwise, an ideal sigmoid voltammogram would be expected, consistent with a steady-state operation of the biocatalyst as the electron flow increases to its limiting value with the increasing potential,

where the current reaches a plateau.[18, 75] However, if the product formation is slowed down, then the acceptance of electrons by the biocatalysts may also slow down, and until the substrate is completely transformed no further electron flow occurs.[76]

Considering the different stoichiometry of the heme ET reaction (n_e=1) and that of bioelectrocatalytic reduction of O_2 ($4e^-$), proceeding stepwise, through the formation of superoxide anion $O_2^{\bullet-}$ and H_2O_2 as intermediate products,[10, 77] several reaction limiting steps, from heme protonation to inhibition of the reaction by the intermediates, can be considered, the gating of ET also contributing to the catalysis efficiency. The most interesting is the transformation of the peak-shaped voltammogram to a sigmoid one for NH_2-terminated SAMs shorter than C11, for which significant conformational changes in the protein active site have been earlier discussed (Figure 8A versus 8B). The apparent efficiency of bioelectrocatalysis on the C_6NH_2, for which a significant increase both in the heme redox potential and heterogeneous ET rate is detected, exceeds four-fivefold that on the C_5COOH-SAM, and the reaction rate appears now to be limited by a process different from that in trHb-*Bs* on the COOH-SAMs. Those data indirectly support our conclusion on different sensitivity of trHb-*Bs*, orientated on SAM-modified electrodes either via its NH_2- or COOH-bearing domains, to the EDL and interfacial stimuli, resulting in protein changes that differently affect ET mechanisms and, as a result, ligand binding and reactivity.

Thus, we suggest that electrochemically interrogated here ET reactions of trHb-*Bs* covalently attached either to amine- or carboxyl-terminated SAM (n<16) on gold, are gated by preceding reactions, which may be proton transfer and/or interfacial conformational changes, induced in the EDL and exhibited via formal potential and ET rate changes. The gated ET reactions of trHb-*Bs* are sensitive to the properties of the surface the protein interacts with and thus to the protein interfacial orientations. That may be of immediate biological relevance and contribute to understanding the regulative mechanisms of the ET reactions proceeding at the protein-protein charged interfaces. It is worth to mention, that such variations in redox properties have been never observed with for example significantly less stable against denaturation cyt *c*.[24, 67, 68] They are generally quite unexpected in otherwise extremely stable trHb-*Bs*, unless they have certain biological implications. The exact functional role of trHb-*Bs* in bacteria is still unclear; the discussed biological functions may include redox sensing and transmission of environmental signals via protein-protein interactions.[7, 41, 42] A bioelectronic *in vivo* modulation of the protein reactivity with its partner molecules through the interactions via protein domains, which sensitivity to environmental actions differs, may then form the mechanistic basis for biological reactivity of trHb-*Bs* in biological redox signalling and actuating processes.

4. Conclusions

Here, ET reactions of the bacterial truncated hemoglobin, trHb-*Bs*, presumably involved in oxygen and other ligand sensing reactions and signal transduction in bacteria, were electrochemically studied. ET properties of trHb-*Bs* covalently attached to either COOH- or NH_2-terminated C16-C2 alkanethiol SAMs on gold strongly depend on the nature of SAM and, correspondingly, protein orientations. While on C16 variations in ET rates for different protein orientations were insignificant, on shorter alkanethiols, a strong shift in the formal redox potential of the heme, most pronounced on NH_2-SAMs, up to 142 mV versus 31 mV on COOH-SAMs, was detected, with the heterogeneous ET rate constant k_s of 789 and 110 s^{-1}, correspondingly, after extrapolation to the SAM zero length. The ET kinetics was not limited by the electron tunnelling through the alkanethiol SAMs but was gated by the preceding reactions, implying strong conformational changes in the heme active site of the protein induced in the electric field of a higher strength and possible interfacial conformational changes, both depending on the charge of alkanethiol SAMs. The observed selective electrostatic modulation of the ET properties of trHb-*Bs* at charged interfaces may be of immediate biological relevance and suggest the involvement a correspondingly charged redox partners operating as messengers in biological ET-related signalling by trHb-*Bs* and actuation of related biological processes.

Acknowledgements

The work was supported by the Danish Council for Independent Research, Natural Sciences (FNU), project number 11-107176, and the Crafoord Foundation and the Carl Tryggers foundation (grant to CVW).

Notes and references

[a] Interdisciplinary Nanoscience Center (iNANO), Science and Technology, Aarhus University, Gustav Wieds Vej 1590-14, DK-8000 Aarhus C, Denmark.

[b] Department of Biology, Lund University, Sölvegatan 35, SE-223 62 Lund, Sweden.

† Electronic Supplementary Information (ESI) available: Additional CV, SWV and DPV data and details of the theoretical calculations. See DOI: 10.1039/b000000x/

1. D. G. Nicholls and S. J. Ferguson, *Bioenergetics 3*, Academic Press, Elsevier Science, Amsterdam, 2002.
2. M. R. Wasielewski, *Chem. Rev.*, 1992, **92**, 435-461.
3. *Cytochrome c: a multidisciplinary approach*, University Science Books, Sausalito, CA, 1996.
4. O. Yehezkeli, R. Tel-Vered, D. Michaeli, I. Willner and R. Nechushtai, *Photosynth. Res.*, 2014, **120**, 71-85.
5. M. Kato, J. Z. Zhang, N. Paul and E. Reisner, *Chem. Soc. Rev.*, 2014, **43**, 6485-6497.
6. M. K. Chan, *Curr. Opinion Chem. Biol.*, 2001, **5**, 216-222.
7. M.-A. Gilles-Gonzalez and G. Gonzalez, *J. Inorg, Biochem.*, 2005, **99**, 1-22.

8. K. R. Rodgers, *Curr. Opin. Chem. Biol.*, 1999, **3**, 158-167.
9. M. Paoli, J. Marles-Wright and A. Smith, *DNA Cell Biol.*, 2002, 271-280.
10. L. Giangiacomo, A. Ilari, A. Boffi, V. Morea and E. Chiancone, *J. Biol. Chem.*, 2005, **280**, 9192-9202.
11. J. B. Wittenberg, Bolognesi, M., Wittenberg, B.A., Guertin, M., *J. Biol. Chem.*, 2002, **277**, 871-874.
12. G. Wu, L. M. Wainwright and R. K. Poole, *Adv. in Microb. Physiol.*, 2003, **47**, 255-310.
13. K. Shikama and A. Matsuoka, *Crit. Rev.Biochem.Mol. Biol.*, 2004, **39**, 217-259.
14. M. Milani, A. Pesce, M. Nardini, H. Ouellet, Y. Ouellet, S. Dewilde, A. Bocedi, P. Ascenzi, M. Guertin, L. Moens, J. M. Friedman, J. B. Wittenberg and M. Bolognesi, *J. Inorg. Biochem.*, 2005, **99**, 97-109.
15. F. A. Armstrong and G. S. Wilson, *Electrochim. Acta*, 2000, **45**, 2623-2645.
16. F. A. Armstrong, *Encyclopedia of Electrochemistry*, 2002, **9**, 11, 13-29.
17. Ferapontova E.E., Shleev S., Ruzgas T., Stoica L., Christenson A., Tkač J., Yaropolov A.I. and Gorton L., in *Electrochemistry of Nucleic Acids and Proteins: Towards Electrochemical Sensors for Genomics and Proteomics*, ed. F. S. Emil Paleček, J. Wang, Elsevier B.V., 2006, vol. 1, pp. 517-598.
18. C. Léger and P. Bertrand, *Chem. Rev.*, 2008, **108** 2379–2438.
19. E. Fernandez, J. T. Larsson, K. J. McLean, A. W. Munro, L. Gorton, C. von Wachenfeldt and E. E. Ferapontova, *Electrochim. Acta*, 2013, **110** 86-93.
20. R. Andrue, E. E. Ferapontova, L. Gorton and J. J. Calvente, *J. Phys. Chem. B.*, 2007, **111**, 469-477.
21. E. E. Ferapontova, *Electroanalysis*, 2004, **16**, 1101-1112.
22. M. Sosna, Bonamore A., Gorton L., Boffi A. and E. E. Ferapontova, *Biosens. Bioelectron.*, 2013, **42**, 219-224.
23. K. R. Rogers, *Anal. Chim. Acta*, 2006, **568**, 222-231.
24. S. Song, R. A. Clark, E. F. Bowden and M. J. Tarlov, *J. Phys. Chem.* , 1993, **97**, 6564-6572.
25. Z. Q. Feng, S. Imabayashi, T. Kakiuchi and K. Niki, *J. Chem. Soc., Faraday Trans.*, 1997, **93**, 1367-1370.
26. A. E. Kasmi, J. M. Wallace, E. F. Bowden, S. M. Binet and R. J. Linderman, *J. Am. Chem. Soc.*, 1998, **120**, 225-226.
27. E. Ferapontova and L. Gorton, *Electroanalysis*, 2003, **15**, 484-491.
28. E. Ferapontova and E. Dominguez, *Bioelectrochemistry*, 2002, **55**, 127-130.
29. A. V. Kartashov, G. Serafini, M. Dong, S. Shipovskov, I. Gazaryan, F. Besenbacher and E. E. Ferapontova, *Phys. Chem. Chem. Phys.*, 2010, **12**, 10098-10107.
30. S. Shipovskov and E. E. Ferapontova, *Biocat. Biotrans.*, 2008, **26**, 508-518.
31. C. Lei, U. Wollenberger, N. Bistolas, A. Guiseppi-Elie and F. W. Scheller, *Anal. Bioanal. Chem.*, 2002, **372**, 235-239.
32. D. H. Murgida and P. Hildebrandt, *J. Am. Chem. Soc.*, 2001, **123**, 4062-4068.
33. E. E. Ferapontova, T. Ruzgas and L. Gorton, *Anal. Chem.*, 2003, **75**, 4841-4850.
34. E. E. Ferapontova, in *Encyclopedia of Sensors*, eds. C. A. Grimes, E. C. Dickey and M. V. Pishko, American Scientific Publishers, Stevenson Ranch, California, USA, 2006, vol. 10, pp. 391-422.
35. M. J. Tarlov and E. F. Bowden, *J. Am. Chem. Soc.*, 1991, **113**, 1847-1849.
36. A. Avila, B. W. Gregory, K. Niki and T. M. Cotton, *J. Phys. Chem. B.*, 2000, **104**, 2759-2766.
37. J. Wei, H. Liu, A. R. Dick, H. Yamamoto, Y. He and D. H. Waldeck, *J. Am. Chem. Soc.*, 2002, **124**, 9591-9599.
38. H. Yue, D. Khoshtariya, D. H. Waldeck, J. Grochol, P. Hilderbrandt and D. H. Murgida, *J. Phys. Chem. B.*, 2006, **110**, 19906-19913.
39. E. E. Ferapontova and L. Gorton, *Bioelectrochemistry*, 2005, **66**, 55-63.
40. X. Chen, R. Ferrigino, J. Yang and G. M. Whitsides, *Langmuir*, 2002, **18**, 7009-7015.
41. T. A. K. Freitas, J. A. Saito, S. Hou and M. Alam, *J. Inorg. Biochem.*, 2005, **99**, 23-33.
42. H. M. Girvan and A. W. Munro, *J. Biol. Chem.*, 2013, **288**, 13194-13203.
43. A. Dolla, L. Blanchard, F. Guerlesquin and M. Bruschi, *Biochimie*, 1994, **76**, 471-479.
44. F. A. Tezcan, J. R. Winkler and H. B. Gray, *J. Am. Chem. Soc.*, 1998, **120**, 13383-13388.
45. M. Sosna, D. Fapyan and E. E. Ferapontova, *J. Electroanal. Chem.* , 2014, **728** 18-25.
46. Y. Gao and I. Kyratzis, *Bioconjug. Chem.*, 2008, **19**, 1945-1950.
47. S. Komorsky-Lovric and M. Lovric, *Anal. Chim. Acta*, 1995, **305**, 248-255.
48. C. C. Page, C. C. Moser, X. Chen and P. L. Dutton, *Nature*, 1999, **402**, 47-52.
49. C. C. Moser, J. M. Keske, K. Warncke, R. S. Farid and P. L. Dutton, *Nature*, 1992, **355**, 796-802.
50. S. Lörcher, P. Lopes, A. Kartashov and E. E. Ferapontova, *ChemPhysChem*, 2013, **14**, 2112-2124.
51. M. Collinson, E. F. Bowden and M. J. Tarlov, *Langmuir*, 1992, **8**, 1247-1250.
52. E. Laviron, *J. Electroanal. Chem.*, 1979, **101**, 19-28.
53. J. F. Rusling, *Acc. Chem. Res.*, 1998, **31**, 363-369.
54. A. J. Bard and L. R. Faulkner, *Electrochemical Methods - Fundamentals and Applications*, Wiley, New York, 1980.
55. H. O. Finklea, K. Yoon, E. Chamberlain, J. Allen and R. Haddox, *J. Phys. Chem. B.*, 2001, **105**, 3088-3092.
56. S. Georg, J. Kabuss, I. M. Wiedenger, D. H. Murgida, P. Hildebrandt, A. Knorr and M. Richter, *Phys. Rev. E*, 2010, **81**, 046101-046101-046101-046110.
57. R. Campos and E. E. Ferapontova, *Electrochim. Acta*, 2014, **126**, 151-157.
58. A. Abi and E. E. Ferapontova, *J. Am. Chem. Soc.*, 2012, **134**, 14499–14507.
59. R. Campos, A. Kotlyar and E. Ferapontova, *Langmuir*, 2014, **30** 11853–11857.
60. J. J. Wei, H. Liu, K. Niki, E. Margoliash and D. H. Waldeck, *J. Phys. Chem. B.*, 2004, **108**, 16912-16917.
61. V. L. Davidson, *Acc. Chem. Res.*, 2000, **33**, 87-93.
62. L. J. C. Jeuken, *Biochim. Biophys. Acta* 2003, **1604**, 67-76.

63. G. K. Rowe and S. E. Creager, *J. Phys. Chem.*, 1994, **98**, 5500-5507.
64. S. Shipovskov, A. M. Saunders, J. S. Nielsen, M. N. Hansen, Gothelf K.V. and F. E.E., *Biosens. Bioelectron.*, 2012, **37**, 99-106.
65. A. S. Viana, A. H. Jones, L. M. Abrantes and M. Kalaji, *J. Electroanal. Chem.*, 2001, **500**, 290-298.
66. Q. Cheng and A. Brajter-Toth, *Anal. Chem.*, 1995, **67**, 2767-2775.
67. R. A. Clark and E. F. Bowden, *Langmuir*, 1997, **13**, 559-565.
68. H. K. Ly, M. A. Marti, D. F. Martin, D. Alvarez-Paggi, W. Meister, A. Kranich, I. M. Weidinger, P. Hildebrandt and D. H. Murgida, *Phys. Chem. Chem. Phys.*, 2010, **11**, 1225-1235.
69. M. Roncel, J. M. Ortega and M. Losada, *Eur. J. Biochem.*, 2001, **268**, 4961-4968.
70. L. Boechi, P. A. Mañez, F. J. Luque, M. A. Marti and D. A. Estrin, *Proteins: Structure, Function, and Bioinformatics*, 2010, **78**, 962-970.
71. S. Shipovskov, E. E. Ferapontova, I. Gazaryan and T. Ruzgas, *Bioelectrochem.*, 2004, **63**, 277-280.
72. H. A. Heering, J. Hirst and F. A. Armstrong, *J. Phys. Chem. B.*, 1998, **102**, 6889–6902.
73. K. Heffron, C. Leger, R. A. Rothery, J. H. Weiner and F. A. Armstrong, *Biochemistry*, 2001, **40**, 3117–3126.
74. T. D. Rapson, U. Kappler and P. V. Bernhardt, *Biochim. Biophys. Acta - Bioenerg.*, 2008, **1777**, 1319–1325.
75. Y. Shao, J. Wang, H. Wu, J. Liu, I. A. Aksay and Y. Lin, *Electroanalysis*, 2010, **22**, 1027-1036.
76. J. M. Hudson, K. Heffron, V. Kotlyar, Y. Sher, E. Maklashina, G. Cecchini and F. A. Armstrong, *J. Am. Chem. Soc.*, 2005, **127**, 6977-6989.
77. B. Royo, M. Sosna, A. C. Asensio, J. F. Moran and E. E. Ferapontova, *J. Electroanal. Chem.*, 2013, **704**, 67-74.

Table of Content (TOC)